15th World Congress on Computational Mechanics (WCCM-XV)
8th Asian Pacific Congress on Computational Mechanics (APCOM-VIII)
Virtual Congress: 31 July – 5 August 2022
S. Koshizuka (Ed.)

A NEW EFFICIENT METHODOLOGY FOR THE ANALYSIS OF MECHANICAL METAMATERIALS WITH ELASTIC INSTABILITIES

NESTOR ROSSI*, CARLOS G. MÉNDEZ AND ALFREDO E. HUESPE

Centro de Investigación de Métodos Computacionales (CIMEC), UNL, CONICET.
Predio "Dr. Alberto Cassano", Colectora Ruta Nacional 168 s/n, Santa Fe, 3000, Argentina.
https://cimec.conicet.gov.ar/
*e-mail: nrossicabral@gmail.com

Key words: metamaterials, reusable energy manipulation, surrogate model of hysteretic elements, microarchitectures with elastic phase transitions.

Abstract. *This work addresses the analysis of mechanical metamaterials exhibiting, as a distinguishing feature, snap-through instabilities in the elastic regime. Among the various opportunities offered by this feature is the manipulation of the material deformation energy [1] that allows the conception of reusable energy-trapping or energy-dissipation devices [2]. As a task to reach this objective, we present a novel computational methodology for analysing microarchitectures displaying elastic snap-through instabilities. The strategy is based on the construction of a surrogate model that reduces the computational burden if compared with full high-fidelity models of non-linear volumetric finite elements or with non-linear beam elements. The surrogate model opens the possibility to analyse a large number of unit cells of periodic metamaterials with instabilities. In addition, it permits an efficient assessment of different geometrical configurations proving a suitable tool for its use in microarchitecture topology optimization processes. Noting that, in general, existing designs of this class of metamaterials only achieve energy manipulation in a specific predefined loading direction, in this work, and based on the proposed computational technique, we aim at the analysis of reusable multidirectional isotropic energy manipulation. This objective agrees with more realistic uses of metamaterials in which general boundary conditions, typically the loading directions, are not established a priori.*

1 INTRODUCTION

Within the extensive field of metamaterials (composites whose microarchitecture is carefully designed to achieve outstanding effective properties), an abundant literature has been published in recent years aiming at exploring the possibility of incorporating elastic snap-through instabilities as functional mechanisms influencing the material deformation process.

In this context, instability refers to a negative incremental stiffness, which could be leveraged to explore interesting and promising prospects, including extreme damping [3], auxeticity with tunable Poisson's ratio [4], control of resonance frequencies through low effective stiffness [5], pattern formation used to control the functionalities and response of the material [6], vibration control [7] and micro-scale mass sensing [8].

The material with snap-through instability arises as a consequence of the non-convexity of its elastic strain energy. This loss of convexity may be the result of non-linear deformation mechanisms, possibly promoted by the geometric deformation phenomena, happening at a lower scale (micro-scale). In the framework of a phenomenological non-linear elasticity description, the loss of convexity (strictly loss of

rank-one convexity) allows the material to display different stable states of deformation (characterized by positive stiffness) called phases, separated by spinodal regions of unstable states. A typical response of this kind of material with two stable phases and one spinodal region is sketched in Figure 1, where the non-convex strain energy function and the corresponding stress-strain response is depicted. Considering that, for certain load levels, the total potential energy may have multiple local minima, then, heterogeneous states of strain, corresponding to different phases, may coexist with a homogeneous state of stress [9].

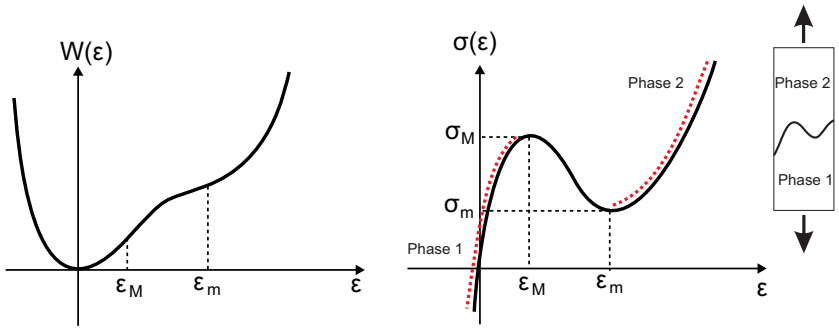

Figure 1: Material with two stable phases and one spinodal region. Left plot: non-convex strain energy $W(\varepsilon)$; central plot: stress (σ)-strain (ε) response; right plot: coexisting phases due to a homogeneous state of stresses.

In the context of applications addressed in the present paper, the remarkable issue about this kind of materials is that, even considering that they are essentially hyperelastic, the phase transitions happening during a loading-unloading process involves an extrinsic mechanical energy dissipation which can be exploited to design adequate devices.

2 MOTIVATION

Our interest in this work resides on the analysis of elastic metamaterials with a periodic microarchitecture, capable of producing repetitively energy dissipation induced by phase transitions that result from multistable elastic systems, typically, from systems displaying snap-through instabilities in more than one direction of loading. Of special importance is to fully understand the connection between the mechanics happening at the micro scale, where phase transition phenomena happens, and the scale where the apparent or effective properties of the material are of interest.

The use of conventional homogenization techniques to reach this objective, an approach that is typically used for analysing and designing mechanical metamaterials in linear elastic regime [10, 11, 12], must be examined carefully for problems displaying instabilities and phase transitions [13]. Note that constant stress states may cause heterogeneous strain states, with the possible coexistence of different phases [9]. On the other hand, the evaluation of the apparent response of the material by including a large number of unit cells also presents a major drawback. An increasing number of unit cells in the model does not only increase the number of (non-linear) equations of the system but also enlarges the number of alternative equilibrium paths and bifurcation points of possible solutions, features being typical of structures with instabilities.

As an alternative to these approaches, we describe in this work a surrogate model that substantially saves computational effort by appropriately capturing the essence of the unstable microarchitecture re-

sponse through a few degrees of freedom. The underlying idea behind this model is to represent the micro-scale *hysteron* (mechanical component causing the snap-through instability, or phase transition, and hysteresis in a closed cycle of loading) through a single 1D finite element endowed with appropriate constitutive law. Although this procedure greatly simplifies the topological complexity of the material structure, it preserves the general characteristic behavior of the material as a whole.

Our approach closely follows an analytical procedure for functionally 1D structures which has been described in [14, 15, 16]. The authors of these works analyze chains of springs in series. The springs show regions with negative stiffness and are modeled with a simplified non-monotonic force-displacement law. Constructive details of the springs leading to such non-linear response at the lower scale are disregarded in this approach. Notably, however their simplicity, such a kind of models is able to capture the same phenomenology obtained with high-fidelity models taking into account the whole microstructure details. Some of these phenomena include: phase transformation and hysteretic material response with serrated loading and unloading plateau [17], energy-absorbing and self-recovering [18], elastic energy trapping without dissipation [19], with a repeatable rate-independent behavior in every case.

The rest of the paper is organized as follows. In section 3, we present the methodology, particularizing it for the case when the hysteron capable of phase transformation is a curved beam. In section 4, we assess the model and compare our results with those obtained by high-fidelity finite element models. Finally, section 5 summarizes the conclusions of the work.

3 METHODOLOGY OF ANALYSIS: A FINITE ELEMENT REDUCED MODEL

Let us consider a periodic metamaterial whose unit cell is constituted by an assembly of hysterons (mechanical elements which may snap in one direction). The present methodology proposes to replace each of these snapping elements by one specially constructed 1D beam finite element.

Beam model

The beam model is formulated according to the kinematic description of the Timoshenko beam, using a small deformation-small displacement theory and a non-linear material. As usual, the kinematics is determined through two fields defined along the beam neutral axis, the vector w is the displacement of the beam neutral axis and θ is the rotation angle of the beam section that in the reference configuration is orthogonal to the neutral axis. The three generalized strains: axial $e(w,\theta)$, curvature $\kappa(w,\theta)$ and shear $\gamma(w,\theta)$ are associated with the three generalized stress resultants: axial N, moment M, and shear Q by appropriate constitutive relations.

The beam finite element implemented in this work has two nodes with three d.o.f. each. These d.o.f. are the nodal axial and transverse displacements (Δ_N, Δ_Q) and the rotation of the original orthogonal section (θ). As usual, the full kinematics of the beam element as well as the generalized stress resultants are determined as functions of these six d.o.f.: axial force $N(\Delta_N, \Delta_Q, \theta)$, moment $M(\Delta_N, \Delta_Q, \theta)$, and shear force $Q(\Delta_N, \Delta_Q, \theta)$.

This type of beam element implemented with a suitable set of constitutive equations is used as a representation of the 1D reduced model of the hysteron element. The reduced model finite element is called *RM-BFE* (Reduced Model-Beam Finite Element) its constitutive equations are discussed below.

Description of the hysteron element studied in this work

In this work, we assume that the hysteron of the metamaterial is constituted by a bistable sinusoidal curved beam with restricted lateral displacements. Figure 2(a) shows the hysteron studied in this work,

and Figure 2(c) depicts a possible microarchitecture unit cell after assemblage. This element displays a phase transition; the system may jump from one stable position to an alternative one when compressed in the vertical direction (snap-through driven condition). Following previous works, see [14, 15, 16], the phase transition effect is conferred to the axial response of the *RM-BFE* element, that is also schematized in Figure 2(a). Thus, to model this effect, the axial stiffness of the *RM-BFE* element is characterized with a non-monotonic response. Instead, as will shown in the following, the bending and shear forces remain monotonic functions with convex energies.

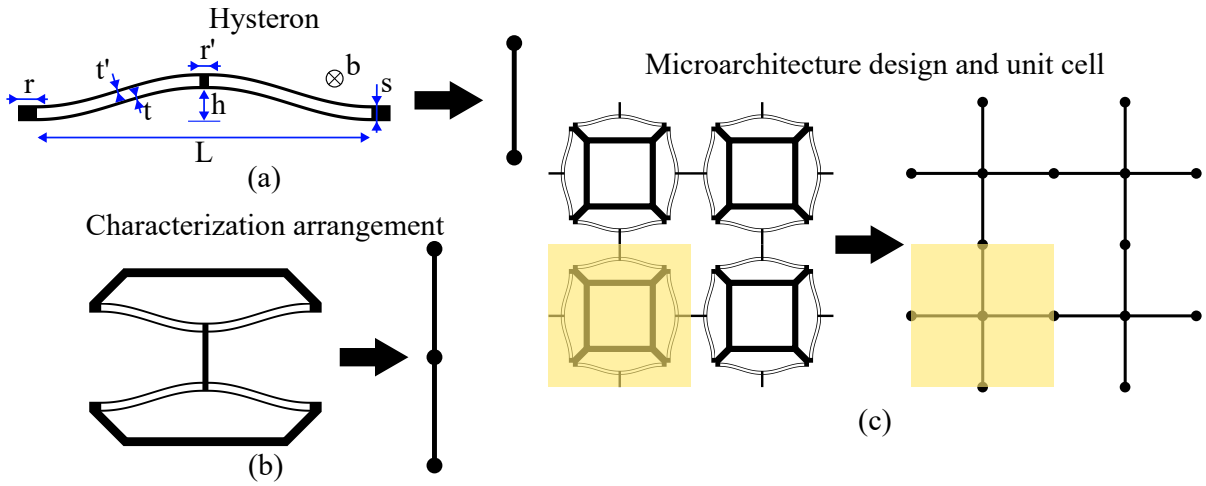

Figure 2: Idealization of the hysteron element as a reduced 1D model. (a) Hysteron with the geometrical dimensions that define its response and a single RM-BFE. (b) Arrangement of two hysterons in series to perform the stiffness characterization of the RM-BFE. (c) Assemblage of four unit cells (yellow shadow) for a square microarchitecture design (proposed by [2, 20])

REMARK. The choice of the transversely loaded curved beam as the element inducing the phase transition (hysteron element) is due to the fact that it has been extensively studied (see [21, 22] and many of the previous references), which allows us to account for an extensive bibliography to compare our results. However, alternative snap elements have been proposed in the literature, such as the mechanism described in [23], where the jump between two stable positions is produced employing rotations, or the mechanism proposed in [24], where phase transitions result from a shear effect. We remark that the present methodology can be easily adapted to represent these alternative hysterons.

3.1 RM-BFE constitutive characterization

The RM-BFE stiffness characterization in our model depends on the kinematical restriction of the curved beam that is subjected to snap-through conditions. In the case studied in the present work, we replicate the configurations reported by [2]. These authors show structures with extrinsic energy dissipation which are functionally 2D with two paired curved beams, one in front of the other, which operate in series. Thus, to obtain suitable results in our model, we characterize the RM-BFE stiffness following a similar configuration that is shown in Figure 2(b), and we call characterization arrangement. The geometrical parameters defining the initial geometry of the curved beam device are specified in Table 1.

To define the three RM-BFE constitutive relations determining the generalized stress resultants N, M,

Table 1: Selected parameters for stiffness characterization [2]. Figure 2 present the graphical description of parameters L, h, t, t', s, r, r', b. The Young modulus of the material of the beams is E_{mat}

$L[mm]$	$h[mm]$	$t[mm]$	$t'[mm]$	$s[mm]$	$r[mm]$	$r'[mm]$	$b[mm]$	$E_{mat}[MPa]$
71	7	0.7	0.7	3.5	4.2	2.1	25	2267

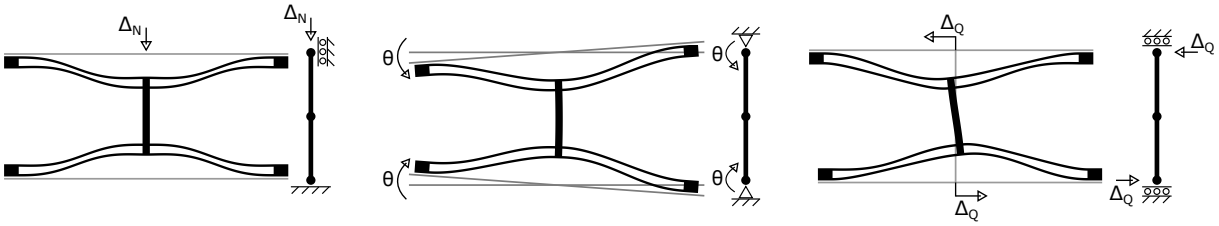

Figure 3: Scheme of the mechanical tests performed on the characterization arrangement of two faced hysterons, to define the constitutive relations of the reduced model

and Q, in terms of the generalized displacements, we assume that they are independent of each other and are only influenced by their respective generalized displacements as follows: $N(\Delta_N)$, $M(\theta)$, $Q(\Delta_Q)$. These three functions are characterized through three separate mechanical test schematized in Figure 3[1].

As a particular case, the expressions reported in [25] are used to characterize the axial stiffness of the RM-BFE element. These authors report the relationship $N(\Delta_N)$, where N is the axial vertical force applied to the curved beam and Δ_N is the vertical displacement of the loading application point, see Figure 3. The function $N(\Delta_N)$ is approximated by a cubic polynomial if the ratio $h/t < 2.31$ is satisfied, or alternatively, it is approximated by a trilinear law. For the parameters indicated in Table 1, we obtain a ratio $h/t = 10$, which implies that the axial force law $N(\Delta_N)$ is trilinear, and it is defined by the position of the following three points (see Figure 4 and equations (43) and (44) in [25]): the first limit load (d_I, N_I), the second limit load (d_{II}, N_{II}), and the second stable configuration with null load $(d_{III}, 0)$:

$$\begin{aligned} N_I &= -18.76\ 10^{-4} MN\ , \\ d_I &= -11.2\ 10^{-4} m\ , \\ N_{II} &= 9.38\ 10^{-4} MN\ , \\ d_{II} &= -134.4\ 10^{-4} m\ , \\ d_{III} &= -139.3\ 10^{-4} m\ . \end{aligned} \tag{1}$$

The moment-curvature law $M(\theta)$ and the shear force-shear displacement $Q(\Delta_Q)$ are instead characterized through results assessed from a high-fidelity finite element model of the curved beams. The outcome of these numerical results are fitted with cubic polynomials. These constitutive relationships are:

$$M = 8.81\ 10^{-5} MNm\ \theta + 71.24\ 10^{-5} MNm\ \theta^3\ , \tag{2}$$

$$Q = 1.624 MN/m\ \Delta_Q + 1.521\ 10^5 MN/m^3\ \Delta_Q^3\ . \tag{3}$$

Figure 4 compares both full- high fidelity finite element results (curves in blue lines) and the reduced model results (curves in red lines) for the tests schematized in Figure 3.

[1] This characterization will be improved in a future work to include the coupling effects between the generalized forces in a generic loading path.

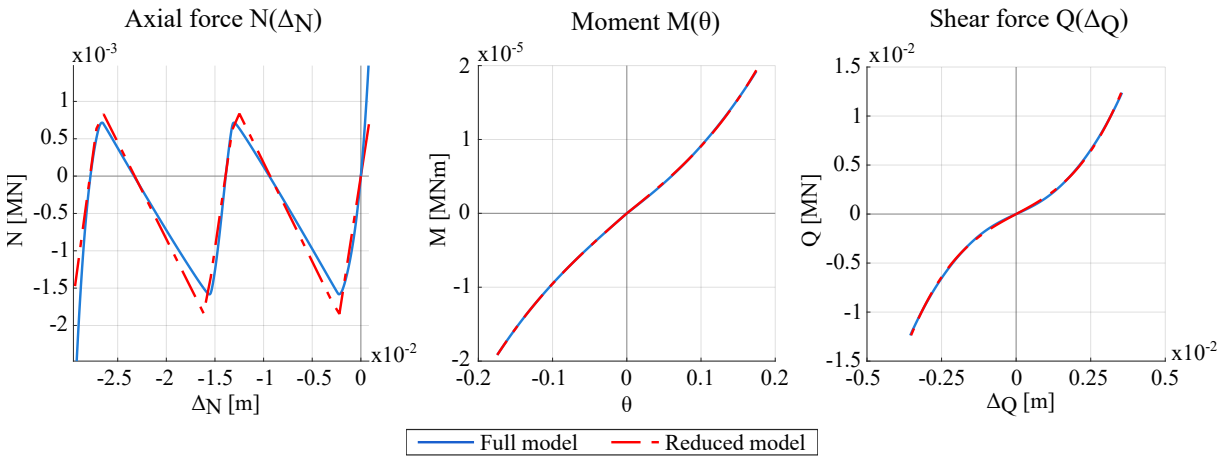

Figure 4: Comparison of the generalized stress resultant curves obtained with a full-high fidelity model (curves in blue lines) and the reduced model endowed by constitutive relationships (1), (2) and (3) (curves in red lines)

3.2 Iterative scheme to solve the balance equations

A critical aspect of the numerical methodology used in this work to obtain the balance equation solutions in structures having a rather large number of hysterons is to choose a suitable iterative scheme. As usual, convergence of the iterative scheme strongly depends on the structural stiffness matrix, which, in the present type of (non-convex) problems is in general non-positive definite. This condition implies that a Newton-Raphson scheme is not an adequate procedure for solving the equation system. Alternatively, to override this problem, we choose a BFGS method together with a line search technique satisfying the Wolfe conditions. This guarantees that the (secant) stiffness matrix is at all times positive definite. For major details see [26].

4 RESULTS

We replicate the results of two 2D microarchitectures reported in [2]. The numerical assessments of the simulated specimens are obtained with the RM-BFE model. The objective of the present assessment is to show the potentiality of the methodology.

The tests are performed on the S-type (S for square type) and T-type (T for triangular type) cellular materials. Both configurations are depicted in Figure 5. The original unit cells designed and tested by [2] and the reduced model unit cells are shown in the same figure. This figure clarifies the association that we introduce between every hysteron, in the original structure, and the individual RM-BFE element. Also, the figure shows the colour code used to report the results. Beams in red indicates that the RM-BFE element remains in phase 1, the stable low deformation phase, while beams in blue indicates that the RM-BFE element has transitioned to phase 2, the stable phase of high deformation.

4.1 Analysis of functionally multidirectional materials

Uniaxial, quasi-static, compressive load-unload tests are performed in the two types of structures. A random variability of 1% is imposed in the t geometrical parameter defining the geometry of the curved beam, see Figure 2. This geometrical perturbation is introduced to avoid convergence problems in the

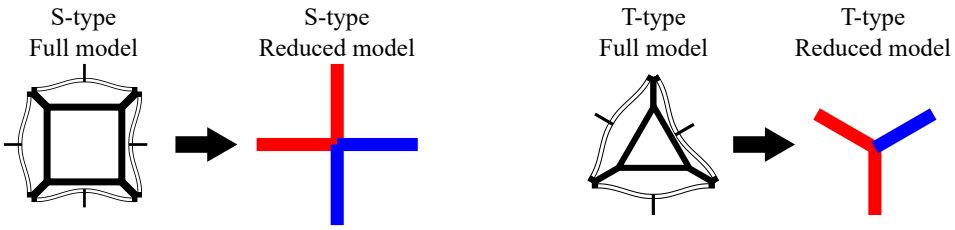

Figure 5: Unit cells of Zhang et al. [2]. S-type (on the left) and T-type (on the right) cellular materials and the corresponding reduced model.

numerical iterative algorithm. This magnitude of variation does not affect notoriously the results and also approximates manufacturability errors.

Following the nomenclature established in [2], in addition to the type of microstructure (S-type or T-type), an angle is given in curly brackets to fully characterize the test. This angle indicates the inclination between a system of local axes attached to the microstructure and the load direction. In all cases, the load is vertically imposed, and the microstructure is rotated accordingly with the indicated angle. Note that both types of microarchitectures have symmetry axes. Therefore, the loading rotation angle conform an eqivalence class. Then, for conciseness, we sometimes only refer to one element of the class.

Figure 6 displays the simulation results of the S-type configuration loaded in the direction $\{0°,90°\}$. Figure 7 shows the results of the S-type at load direction $\{45°,135°\}$. Figure 8 shows the results of the T-type configuration loaded along the direction $\{0°,60°,120°\}$, and Figure 9 displays the results of the T-type at load direction $\{30°,90°,150°\}$. The plots in these figures display the load-displacement curves in closed cycles of loading, as well as three snapshots of the deformation pattern at sequential loading stages. Note in the force vs displacement plots, the hysteresis loop generated when subjected to a closed loading cycle. The area enclosed by the hysteresis loop represent the extrinsic energy dissipation of each system. Compare these results with Figures 3 to 7 of [2] (note that in our graphics compression loads have negative sign).

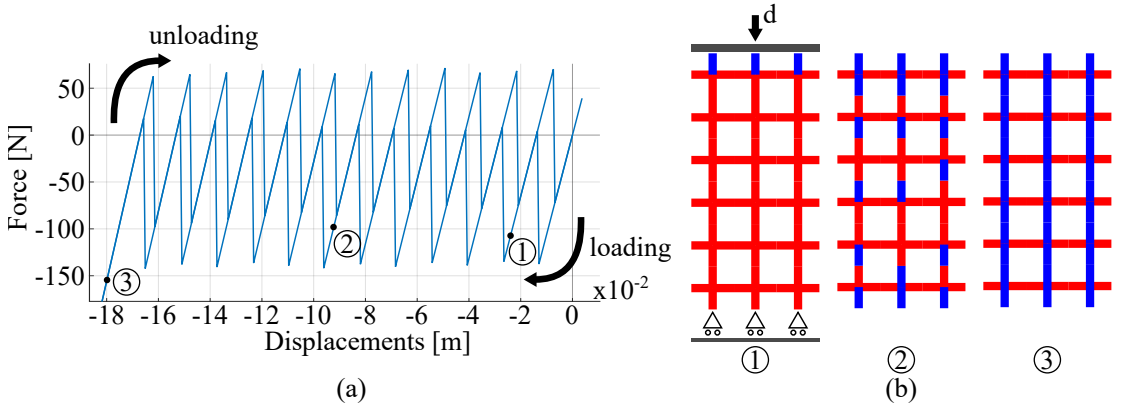

Figure 6: S-type configuration. Load direction $\{0°,90°\}$. (a) total vertical force vs. displacement of the specimen top (closed loading cycle). (b) sequence of phase transitions at points 1, 2, and 3 accordingly with the position displayed in the left plot.

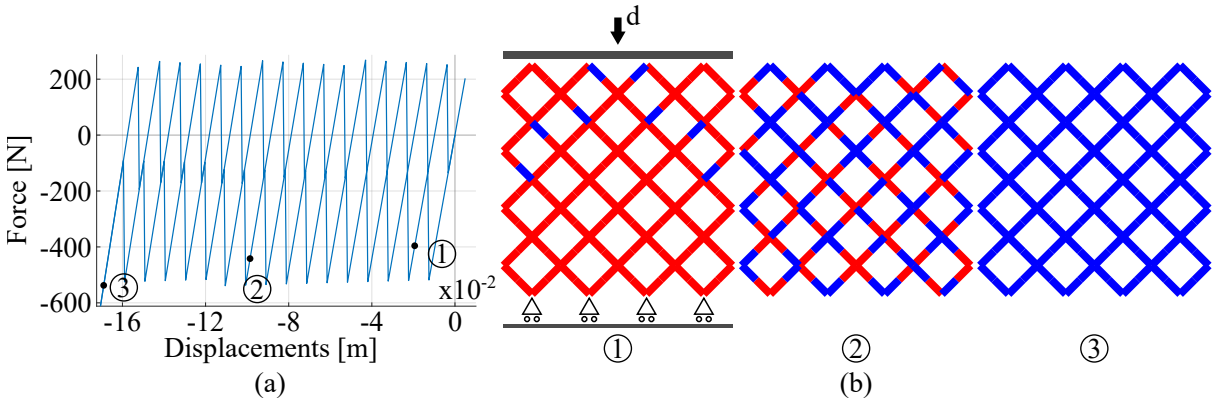

Figure 7: S-type configuration. Load direction $\{45°,135°\}$. (a) total vertical force vs. displacement of the specimen top (closed loading cycle). (b) sequence of phase transitions at points 1, 2, and 3 accordingly with the position displayed in the left plot.

The results of the simulations obtained with the reduced model show good agreement with many important features reported in the experimental and results of [2]. The model captures every snapping event (limit loads when a row of the microstructure performs a phase transition), obtaining the correct deformation patterns in every case. Typically, in Figures 6 and 9 (S-type at $\{0°\}$ and T-type at $\{90°\}$ structures), we show that the RM-BFE elements orthogonal to the loading directions do not perform a phase transition. Also, Figure 8 shows that vertical RM-BFE elements in the T-type $\{0°\}$ perform the phase transition first, and subsequently, the inclined ones. Note also the phase transition pattern, like a "V", of the S-type $\{45°\}$ structure in the first snapshot of Figure 7.

Additionally, the model captures the typical serrated loading and unloading plateaus. For the T-type $\{0°\}$ structure, it also predicts two different levels of plateaus corresponding to the orientation of the hysteron elements subjected to phase transformation.

The reduced model quantitatively predicts correct displacement values, both for individual snapping events and at the maximum loading condition reached in the simulation, when the dissipation capacity is exhausted. However, limit load values are not sufficiently well predicted. This may be mainly due to the following two reasons:

i) First, Qiu's law [25], which is used to characterize the axial response of the RM-BFE element, assumes that curved-beams are perfectly fixed in the lateral direction. This type of constraint is difficult to manufacture and obtain in assembled microstructures, since the interior frames constraining the lateral displacements of the curved-beams are not infinitely stiff. The lateral restriction compliance, even being small, generates a decrease in the hysteron limit load which may explain part of the difference between the numerical and experimental limit loads in the S-type $\{0°\}$ structure.

ii) The second reason may be associated with the performance of the model. The performance may be particularly affected when the RM-BFE elements are not aligned to the loading direction. Considering the RM-BFE constitutive law adopted for the bending and shearing effects, larger inclinations of the loading direction respect to the RM-BFE longitudinal axis induce a decreasing effect of the axial response, and the total energy of the system tends toward convexity. Thus, the capacity of the system to dissipate energy decreases. It is worth mentioning that capturing the right limit loads in RM-BFE elements under inclined loads is a challenge, see for example [2].

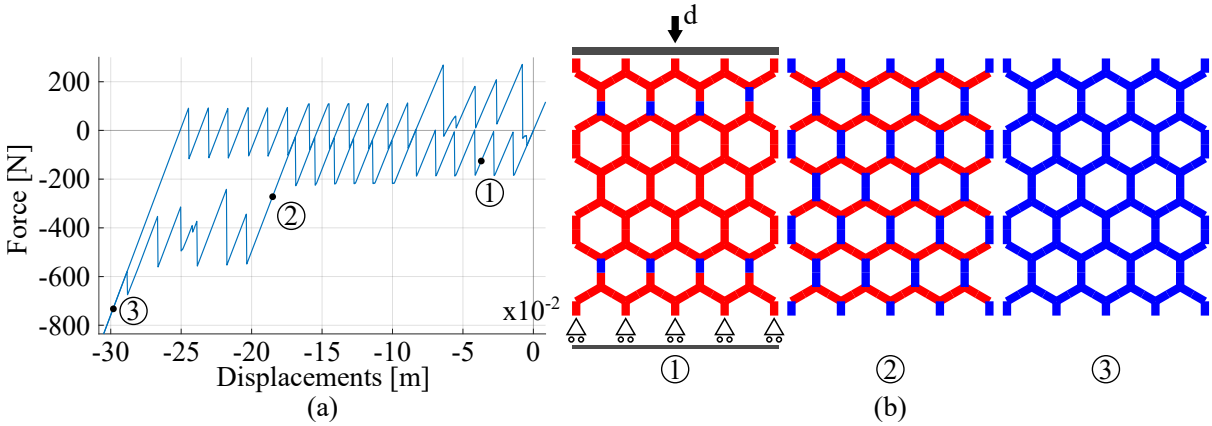

Figure 8: T-type configuration. Load direction $\{0°,60°,120°\}$. (a) total vertical force vs. displacement of the specimen top (closed loading cycle). (b) sequence of phase transitions at points 1, 2, and 3 accordingly with the position displayed in the left plot.

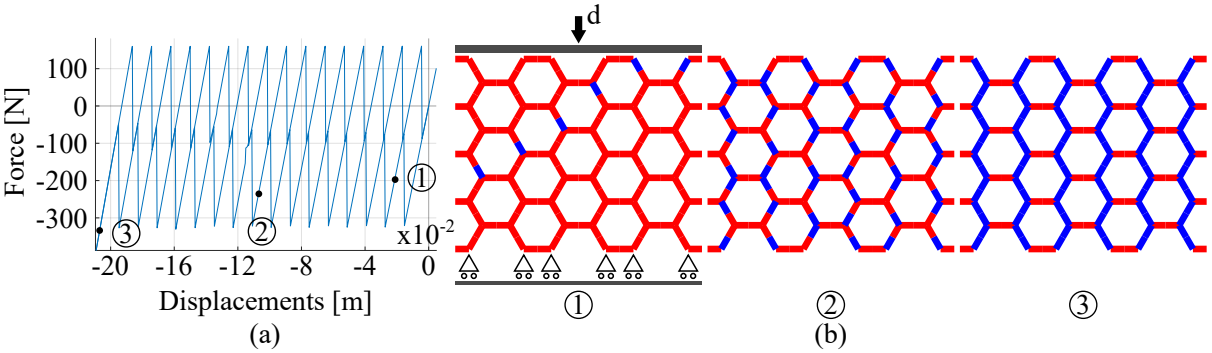

Figure 9: T-type configuration. Load direction $\{30°,90°,150°\}$. (a) total vertical force vs. displacement of the specimen top (closed loading cycle). (b) sequence of phase transitions at points 1, 2, and 3 accordingly with the position displayed in the left plot.

4.2 Isotropy of the energy dissipation

From the equilibrium paths displayed in the plots of Figures 6–9, we estimate the averaged dissipated energy per RM-BFE element for both configurations (S and T-types) along the two possible axes of symmetry.

However, since the effectiveness of the structural energy dissipation depends on the number of hysterons in series, we initially perform a convergence analysis by increasing the number of rows (hysterons in series) in the specimen that perform a snapping event until the average dissipation is stabilized. The attained results for S-type loaded at $\{0°\}$ and $\{45°\}$ and for T-types of configurations loaded at $\{0°\}$ and $\{90°\}$ are plotted in Figure 10(a), and the stabilized converged values of average dissipated energy per RM-BFE are displayed in the polar diagram of Figure 10(b).

In relation with the tendency of the model to overestimate load values if elements are inclined, it is likely that the dissipated energy is also overestimated, particularly affecting S-type 45 and T-type 0, since

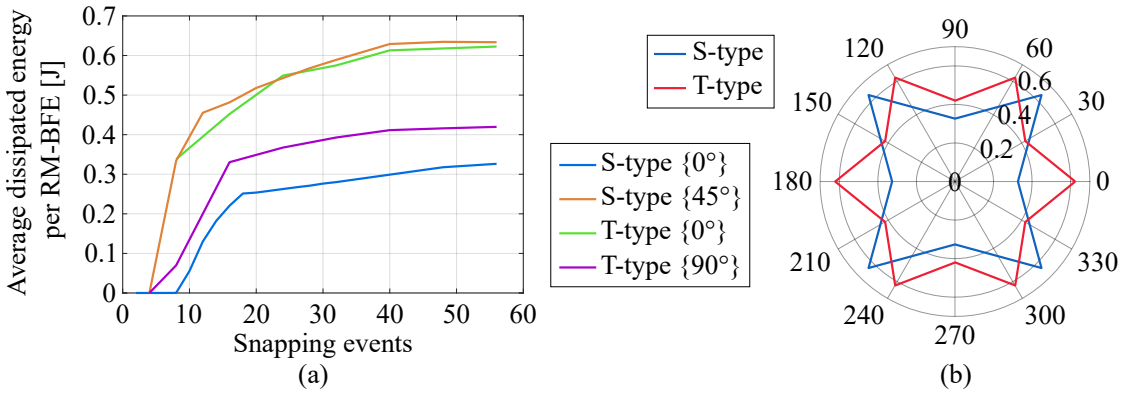

Figure 10: Energy dissipation for different loading directions. (a) Convergence of the average dissipated energy per RM-BFE as a function of the amount of snapping events (or hysterons in series), for both S-type and T-type microstructures and in two loading directions. (b) Average dissipated energy as a function of the loading direction for both designs.

their elements have greater inclinations.

4.3 Computational efficiency

To show the potentiality of the reduced model regarding computational cost, we compare the required CPU times to perform the simulations of the test discussed in Figure 4, and using either the High-Fidelity finite element model (HF) (blue curves in Figure 4) or the Reduce Model (RM) (red curves in Figure 4). Table 2 shows the required CPU time, in seconds, to perform the full analysis of $N(\Delta_N)$, $M(\theta)$, and $Q(\Delta_Q)$ using both HF and RM models.

Table 2: Elapsed times in seconds to perform the analyses of $N(\Delta_N)$, $M(\theta)$, and $Q(\Delta_Q)$ using either the High-Fidelity finite element model (HF) or the surrogate model (RM) (simulated tests correspond to those displayed in Figure4)

$N(\Delta_N)$ HF	$N(\Delta_N)$ RM	$M(\theta)$ HF	$M(\theta)$ RM	$Q(\Delta_Q)$ HF	$Q(\Delta_Q)$ RM
237.6	4.4	51.0	0.7	42.5	1.4

The drastic CPU saving time shown by the RM model, in comparison to that demanded by the HF model, is due to the drastic dimensionality reduction of the problem. The HF model uses 1.6×10^5 d.o.f. compared against only one finite element and six d.o.f. used by the RM approach. [2]

5 CONCLUSIONS

We present an efficient tool for the analysis of metamaterials displaying snap-through instabilities and phase transformation. Although the challenges of modeling mechanical structural response with large number of instabilities (including bifurcation points, multiple solutions, etc.) are still present, the reduced model here reported provides a computational robustness increase when a rather large number

[2] Additionally, note that the HF model is defined in terms of a full non-linear geometry and material theory, whereas the RM model is defined in terms of small deformation and small strain theory with a non-linear constitutive model.

of hysterons are simulated.

The hysteron that is chosen to assess the reduced model consists of a bistable curved/beam. However, we hold that the reported procedure to define the reduced model is transparent to the mechanism introducing the snap-through instability phenomenon. Therefore, the model could be quite straightforwardly generalized for hysterons generated by different mechanical devices.

Furthermore, this reduced model displays an acceptable qualitative predictive capacity regarding cyclic loading paths. This predictive capacity includes patterns of phase transformations, serrated plateaus in the load-displacement plots with hysteresis, and energy dissipation decrease when the hysteron is not aligned with the loading direction.

Quantitatively, the model correctly predicts displacement values, although overestimates load values. This drawback could be overridden by improving the constitutive description of the RM-BFE element. This is a work in development.

The saved computational cost makes this methodology especially suitable for its use in an optimization process where different configurations of hysterons could be tested. This aspect of the problem is also to be explored by the authors in the near future.

ACKNOWLEDGMENT

Nestor Rossi gratefully acknowledges the support received by AUIP (Asociación Universitaria Iberoamericana de Postgrado) under the program of academic mobility between the institutions associated to the AUIP. This research has been supported with grants provided by CONICET, the National University of Litoral, and the fund from ANPCyT: PICT-2020-SERIEA-02793, Argentina.

REFERENCES

[1] Kochmann, D.M. and Bertoldi, K. Exploiting microstructural instabilities in solids and structures: from metamaterials to structural transitions. *Appl. Mech. Reviews.* (2017) **69**(5).

[2] Zhang, Y., Restrepo, D., Velay-Lizancos, M., Mankame, N.D. and Zavattieri, P.D. Energy dissipation in functionally two-dimensional phase transforming cellular materials. *Scientific reports.* (2019) **9**(1):1–11.

[3] Lakes, R.S., Lee, T., Bersie, A. and Wang, Y.C. Extreme damping in composite materials with negative-stiffness inclusions. *Nature.* (2001) **410**(6828):565–567.

[4] Bertoldi, K., Reis, P.M., Willshaw, S. and Mullin, T. Negative Poisson's ratio behavior induced by an elastic instability. *Advanced materials.* (2010) **22**(3):361–366.

[5] Wojnar, C.S. and Kochmann, D.M. A negative-stiffness phase in elastic composites can produce stable extreme effective dynamic but not static stiffness. *Philos. Mag.* (2014) **94**(6):532–555.

[6] Shan, S., Kang, S.H., Wang, P., Qu, C., Shian, S., Chen, E.R. and Bertoldi, K. Harnessing multiple folding mechanisms in soft periodic structures for tunable control of elastic waves. *Advanced Functional Materials* (2014) **24**(31):4935–4942.

[7] Johnson, D.R., Harne, R.L. and Wang, K.W. A disturbance cancellation perspective on vibration control using a bistable snap-through attachment. *Journal of Vibration and Acoustics* (2014) **136**(3).

[8] Harne, R.L. and Wang, K.W. A bifurcation-based coupled linear-bistable system for microscale mass sensing. *Journal of Sound and Vibration* (2014) **333**(8):2241–2252.

[9] Abeyaratne, R. and Knowles, J. K. *Evolution of phase transitions: a continuum theory*. Cambridge University Press, (2006).

[10] Rossi, N., Podestá, J.M., Bre, F., Méndez, C.G. and Huespe, A.E. A microarchitecture design methodology to achieve extreme isotropic elastic properties of composites based on crystal symmetries. *Structural and Multidisciplinary Optimization* (2021) **63**(5):2459–2472.

[11] Rossi, N., Yera, R., Mendez, C.G., Toro, S. and Huespe, A.E. Numerical technique for the 3D microarchitecture design of elastic composites inspired by crystal symmetries. *Computer Methods in Applied Mechanics and Engineering* (2020) **359**:112760.

[12] Yera, R., Rossi, N., Méndez, C.G. and Huespe, A.E. Topology design of 2D and 3D elastic material microarchitectures with crystal symmetries displaying isotropic properties close to their theoretical limits. *Applied Materials Today* (2020) **18**:100456.

[13] Nuñez-Labielle, A., Cante, J., Huespe, A.E. and Oliver, J. Towards shock absorbing hyperelastic metamaterial design.(I) Macroscopic scale: Computational shock-capturing. *Computer Methods in Applied Mechanics and Engineering*, (2022) **393**:114732.

[14] Puglisi, G. and Truskinovsky, L. Mechanics of a discrete chain with bi-stable elements. *J. Mech. Phys. Solids.* (2000) **48**(1):1–27.

[15] Puglisi, G. and Truskinovsky, L. Rate independent hysteresis in a bi-stable chain. *J. Mech. Phys. Solids.* (2002) **50**(2):165–187.

[16] Puglisi, G. and Truskinovsky, L. Thermodynamics of rate-independent plasticity. *J. Mech. Phys. Solids.* (2005) **53**(3):655–679.

[17] Restrepo, D. and Mankame, N.D. and Zavattieri, P.D. Phase transforming cellular materials. *Extreme Mechanics Letters.* (2015) **4**:52–60.

[18] Frenzel, T., Findeisen, C., Kadic, M., Gumbsch, P. and Wegener, M. Tailored buckling microlattices as reusable light-weight shock absorbers. *Advanced Materials.* (2016) **28**(28):5865–5870.

[19] Shan, S., Kang, S.H. Raney, J.R., Wang, P., Fang, L., Candido, F., Lewis, J.A. and Bertoldi, K. Multistable architected materials for trapping elastic strain energy. *Advanced Materials.* (2015) **27**(29):4296–4301.

[20] Ren, C., Yang, D. and Qin, H. Mechanical performance of multidirectional buckling-based negative stiffness metamaterials: an analytical and numerical study. *Materials.* (2018) **11**(7):1078.

[21] Correa, D.M., Klatt, T., Cortes, S., Haberman, M., Kovar, D. and Seepersad, C. Negative stiffness honeycombs for recoverable shock isolation. *Rapid Prototyping Journal.* (2015).

[22] Ha, C.S., Lakes, R.S. and Plesha, M.E. Design, fabrication, and analysis of lattice exhibiting energy absorption via snap-through behavior. *Materials & Design.* (2018) **141**:426–437.

[23] Jeong, H.Y., An, S.C., Seo, I.C., Lee, E., Ha, S., Kim, N. and Jun, Y.C. 3D printing of twisting and rotational bistable structures with tuning elements. *Scientific reports.* (2019) **9**(1):1–9.

[24] Liu, S., Azad, A.I. and Burgueño, R. Architected materials for tailorable shear behavior with energy dissipation. *Extreme Mechanics Letters.* (2019) **28**:1–7.

[25] Qiu, J., Lang, J.H. and Slocum, A.H. A curved-beam bistable mechanism. *Journal of microelectromechanical systems.* (2004) **13**(2):137–146.

[26] Nocedal, J. and Wright, S.J. *Numerical optimization*. Springer, (1999).